Clay Minerals (2023), **58**, 19–25
doi:10.1180/clm.2023.6

CAMBRIDGE UNIVERSITY PRESS

Article

Effects of clay activation and amine chain length on silica–palygorskite heterostructure properties

Lilya Boudriche[1]*, Faïza Bergaya[2] and Amel Boudjemaa[1]

[1]Centre de Recherche Scientifique et Technique en Analyses Physico-Chimiques, BP 384 Bou-Ismail, RP 42004 Tipaza, Algeria and [2]Interface, Confinement, Matériaux et Nanostructures (ICMN), CNRS – Université d'Orléans, 1b rue de la Férollerie, 45071 Orléans, France

Abstract

Various approaches have been used for the preparation of heterostructured materials based on clay minerals, with numerous potential applications offered by the resulting functional materials. In this study, a fibrous clay mineral (palygorskite) and a tetraethyl orthosilicate reagent were used to obtain silica–palygorskite heterostructures. The aim was to highlight the influence of two factors during the preparation process: the effect of acid activation pre-treatment of the palygorskite with HCl and the effect of varying the length of the amine chains used – dodecylamine and butylamine – on the formation and development of silica nanoparticles on the surface of the palygorskite fibres. The silica–palygorskite heterostructures were obtained after the removal of the organic templates by calcination at 500°C. The textural and structural properties of the silica–palygorskite heterostructured samples were determined using various experimental characterization techniques, such as X-ray diffraction, transmission electron microscopy, gas adsorption and Fourier-transform infrared spectroscopy. The experimental variables targeted in this study appeared to have a significant effect on the textural properties of the silica–palygorskite heterostructure obtained. The great specific surface area and the mesoporous, microporous and ultramicroporous volumes as determined using nitrogen and/or carbon dioxide gas adsorption confirm the benefit of combining the acid activation pre-treatment of the fibrous clay mineral with the use of a long-chain amine co-surfactant (dodecylamine). The resulting silica–palygorskite heterostucture has a great specific surface area (628 $m^2\ g^{-1}$) and a well-developed total pore network ($V_{N2} = 0.24\ cm^3\ g^{-1}$; $V_{ultra\ (CO2)} = 0.18\ cm^3\ g^{-1}$). This material will be tested for the removal of volatile organic compounds at low concentrations.

Keywords: acid treatment, amine chain length, heterostructure, palygorskite, physicochemical characterizations, silica nanoparticles

(Received 28 September 2022; revised 10 January 2023; Accepted Manuscript online: 27 February 2023; Associate Editor: Chun Hui Zhou)

Porous nanoarchitectures based on clay minerals have been a focus of growing interest in the field of materials science due to their ability to produce nanostructures with beneficial functional and structural properties (Polverejan *et al.*, 2000; Ruiz-Hitzky & Aranda, 2014; Kooli *et al.*, 2017). This multifunctionality supports their use in various fields, notably in environmental remediation *via* the removal of pollutants due to their catalytic and adsorption properties and in the medical field in terms of the development of viable and functional biodevices for biomedical applications, as supports for the controlled release of drugs and in bioimaging (Tobajas *et al.*, 2017; Akkari *et al.*, 2018; Yuan *et al.*, 2018; Yang *et al.*, 2019; Dai *et al.*, 2021; Persano *et al.*, 2021).

Among the clay minerals that have been studied, fibrous clay minerals have taken a prominent place in recent years due to their beneficial properties, such as the presence of silanol groups on the external surfaces of these fibres, which facilitates their assembly with various types of nanoparticle, thus giving great stability to the nanoarchitectures obtained (Belver *et al.*, 2012; Aranda *et al.*, 2018). Moreover, the possibility of controlling the size of the pores of these nanostructured materials (Polverejan *et al.*, 2000; Gómez-Avilés *et al.*, 2013; Cecilia *et al.*, 2018) allows various possible applications, particularly in catalysis, environmental remediation and energy production, among others (Guggenheim & Krekeler, 2011; Ruiz-Hitzky & Aranda, 2014). Depending on the synthesis method used, the resulting functional nanostructures can be used as antibacterials, adsorbents of pollutants, ion exchangers and magnetic sensors, etc. (González-Alfaro *et al.*, 2011; Ruiz-Hitzky *et al.*, 2011).

The present study focuses on the possibility of obtaining a heterostructured silica–clay mineral using palygorskite as the starting fibrous clay mineral. Palygorskite belongs to the class of TOT fibrous non-swelling phyllosilicates in which the silica tetrahedra are inverted periodically in the tetrahedral sheets, giving rise to channels (Bradley, 1940; Chahi *et al.*, 2002; Suarez & Garcia-Romero, 2006; Boudriche *et al.*, 2010, 2011). Previous research has shown that the combination of the thermal resistance and adsorptive properties of palygorskite with the mechanical reinforcement of silica can offer great potential for various applications, especially from an environmental perspective (Yang *et al.*, 2010; Ruiz-Hitzky *et al.*, 2011; Gómez-Avilés *et al.*, 2013). Moreover, Aranda & Ruiz-Hitzky (2018) reported previously that the characteristics of the heterostructures thus obtained can be affected significantly by various aspects related to the preparation methodology.

The aim of this study is to highlight, through textural, structural, morphological and mineralogical characterizations of the nano-heterostructures obtained, the effects of two experimental

*Email: boud_lil@yahoo.fr

Cite this article: Boudriche L, Bergaya F, Boudjemaa A (2023). Effects of clay activation and amine chain length on silica–palygorskite heterostructure properties. *Clay Minerals* **58**, 19–25. https://doi.org/10.1180/clm.2023.6

parameters: (1) prior activation of the clay mineral with hydrochloric acid (HCl); and (2) variation of the amine chain length on the development of silica nanoparticles around palygorskite fibres.

Experimental

Materials

The raw palygorskite used in this study was extracted from a natural deposit (Ghoufi) located in Algeria (Boudriche *et al.*, 2010; Ouali *et al.*, 2015; Habibi *et al.*, 2018) and has the following average mineralogical formula: $(Si_{7.88}Al_{0.12})O_{20}(Mg_{1.69}Al_{1.71}Fe_{0.43})(OH)_2(K_{0.06}Ca_{0.05}Na_{0.15})(OH_2)_4{\cdot}4H_2O$ (Belaroui *et al.*, 2018). All other chemicals used, such as hexadecyltrimethylammonium bromide ($C_{19}H_{42}BrN$ or HDTABr), butylamine ($C_4H_{11}N$ or BTA), dodecylamine ($C_{12}H_{27}N$ or DDA), sodium chloride (NaCl), HCl and tetraethylorthosilicate ($SiC_8H_{20}O_4$ or TEOS), were of analytical grade, were manufactured by Sigma-Aldrich (France) and were used without further purification.

Synthesis method

The raw palygorskite was milled and sieved to <1 mm, and this sample is referred as Pal. The Pal sample was first treated with HCl (0.5 M) at a 1/10 (solid/liquid) ratio at 100°C for 6 h to remove impurities such as carbonates. Then it was mixed with an excess of NaCl solution (1 M) to induce cation exchange with Na^+. This cation-exchange step was repeated six times to ensure complete exchange. The sample obtained was then washed several times with hot distilled water to remove the chloride anions and finally dried at 100°C for 24 h. The treated sample obtained is referred as Pal-T.

The first step of synthesis is the formation of an organo-palygorskite by adding 3 g of Pal-T to 300 cm^3 of 0.1 M HDTABr surfactant solution (long-chained quaternary ammonium cations). This dispersion was stirred for 24 h at 50°C to allow the sodium cations to be replaced by the organic surfactant cations. Then, the excess alkylammonium salt was removed *via* repeated washing with hot distilled water and centrifugation of the supernatant until an $AgNO_3$ test indicated the absence of halide anions. The resulting solid was air-dried. The organo-palygorskite thus obtained is referred to as OPal-T.

In the next step, a neutral amine co-surfactant, DDA or BTA, with a silica precursor TEOS were added to 1 g of OPal-T in the amounts corresponding to an OPal-T/neutral amine/silica precursor ratio of 1/20/150. After 4 h of stirring at room temperature, the solid component was recovered by filtration and air dried. The samples obtained are referred to as OPal-T/DDA/TEOS and OPal-T/BTA/TEOS.

After calcination at 500°C for 6 h under airflow (heating rate 1°C min^{-1}), silica–palygorskite heterostructures with co-surfactant BTA and DDA were obtained, which are referred to as SPal-T-BTA or SPal-T-DDA, respectively (Fig. 1).

Characterization techniques

X-ray diffraction (XRD) traces were recorded using a PANalytical XPERT-PRO diffractometer (New Jersey, USA) with Cu-*K*α radiation (λ = 1.5405 Å). The powdered samples were placed without any pre-treatment in a horizontal sample holder. The instrument was operated at 45 kV and 40 mA with a step size of 0.02°2θ over a range of 2–45°2θ.

The specific surface area (SSA) and mesoporous and microporous volumes were calculated using gas adsorption (N_2, CO_2). The samples were outgassed overnight at 120°C under vacuum and their porosity was characterized by N_2 and CO_2 adsorption, respectively, at −196°C and 0°C (Autosorb-1, Quantachrome, FL, USA). The total pore volume was estimated from the amount adsorbed at $P/P_0 = 0.95$. The microporous and the mesoporous volumes were determined by applying the density functional theory (DFT) method to the N_2 isotherms. The Dubinin–Radushkevich (DR) theory was applied to the CO_2 adsorption isotherm to estimate the ultramicropore volume (diameter <0.7 nm).

Morphology and microtexture were investigated using conventional high-resolution transmission electron microscopy (TEM-FEI CM20, Philips, Germany) operating at 200 kV and at 0.14 nm resolution.

The infrared spectra of SPal were obtained using an Alpha-Bruker (Germany) spectrometer, with Fourier-transform infrared spectroscopy (FTIR) conducted in the range 400–4000 cm^{-1} with a resolution of 2 cm^{-1} and a scan number equal to 32. The attenuated total reflection module was used by placing the sample to be analysed in contact a crystal (diamond) without dilution in KBr.

Results and discussion

Mineralogical analysis

The XRD trace (Fig. 2) of Pal allowed the identification of the following mineralogical phases: palygorskite as the main phase and carbonates in two crystalline forms: calcite ($CaCO_3$) and dolomite ($CaMg(CO_3)_2$). The characteristic reflections of the carbonates

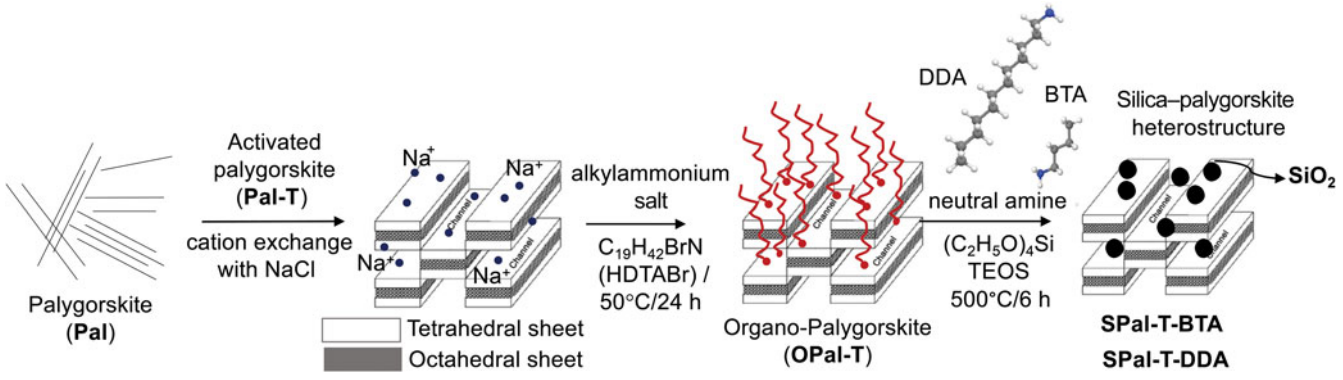

Fig. 1. Schematic illustration of the general procedure followed to prepare the silica–palygorskite heterostructure SPal-T-BTA and SPal-T-DDA.

https://doi.org/10.1180/clm.2023.6 Published online by Cambridge University Press

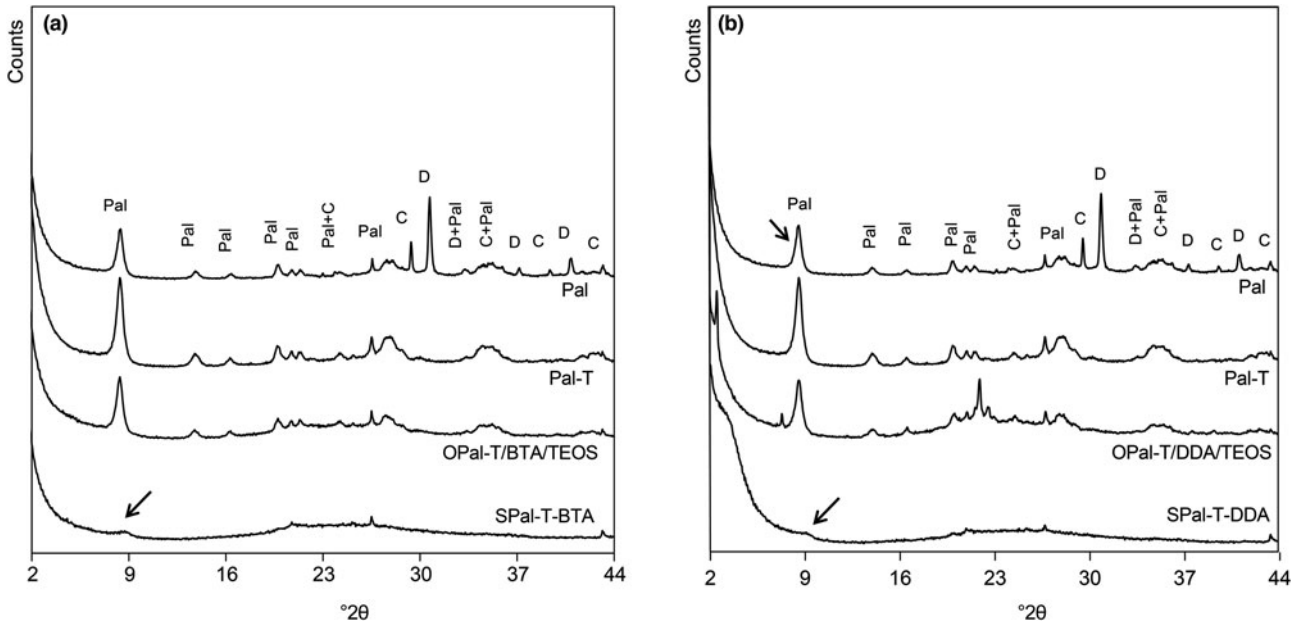

Fig. 2. X-ray diffraction (XRD) traces of raw palygorskite (Pal) and activated palygorskite (Pal-T) with: (a) the silica–palygorskite organo-heterostructure OPal-T/BTA/TEOS and the silica–palygorskite heterostructure SPal-T-BTA; and (b) the silica–palygorskite organo-heterostructure OPal-T/DDA/TEOS and the silica–palygorskite heterostructure SPal-T-DDA. The arrows represent the Pal in the SPal-T-DDA and SPal-T-BTA samples. C = calcite; D = dolomite.

disappear in the XRD trace of Pal-T, with preservation of the crystalline structure of palygorskite after acid treatment, which is in agreement with previous studies (Ouali *et al.*, 2015; Habibi *et al.*, 2018).

The XRD traces of samples OPal-T/BTA/TEOS (Fig. 2a) and OPal-T/DDA/TEOS (Fig. 2b) indicate that the structure of palygorskite was not affected by the silica–palygorskite organo-heterostructure formation step. However, after calcination of these samples at 500°C, corresponding to organic matter removal, the XRD traces of SPal-T-DDA and SPal-T-BTA show the formation of a broad band at 16–37°2θ, attributed to the presence of amorphous silica, which obscures the Pal-T reflections. In addition, a small shift of the characteristic palygorskite reflections from 8.4 to 9.3°2θ was observed, which is attributable either to the insertion of silica gel into the structural channels, which replaced the zeolitic water removed after calcination, or to the existence of a distortion of the structure due to the interaction of SiOH with the nanoparticles formed. A similar observation was noted in previous studies performed on sepiolites (Belver *et al.*, 2013; Aranda & Ruiz-Hitzky, 2018).

In the present case, according to the TEM results (Fig. 3), the disappearance of the characteristic reflections of Pal after calcination during the XRD analysis does not mean that the Pal structure was destroyed, but rather that the Pal surface was covered entirely by a silicic structure.

The XRD trace of SPal-T-DDA revealed the formation of SiO_2 on the surface of the Pal-T fibres (Fig. 2b) with the appearance, in addition to the broad band in the range 16–37°2θ, of a shoulder at ~3.6°2θ, probably due to a more pronounced entanglement and consolidation of the nanostructure between the Pal-T fibres and the long-chain co-surfactant DDA compared to BTA.

Morphological analysis

The TEM microstructural analysis of the Pal sample (Fig. 3) indicated a fibrous morphology with the presence of cubic shapes inserted within the fibres. Energy-dispersive X-ray (EDX) analysis of the fibres and the cubic crystals identified their majority chemical composition (atomic %): Mg (17.67%), Al (8.89%), Si (70.97%) for the fibres and Ca (51.35%) for the cubic crystals (dashed circle in Fig. 3) related to carbonate impurities (calcite and dolomite, as also confirmed by XRD).

The purification of the Pal sample with HCl allowed the removal of the cubic crystals related to carbonate impurities from the Pal sample (Boudriche *et al.*, 2011). After calcination, spherical particles appeared, associated with the formation of a polysiloxane network surrounding the Pal fibres for the SPal-T-BTA and SPal-T-DDA samples. The presence of small particles on the surface of the Pal-T fibres is detectable in the SPal-T-BTA and SPal-T-DDA heterostructures *via* TEM analysis. However, these particles are denser according to EDX analysis (Fig. 4) in SPal-T-DDA sample, forming agglomerates of palygorskite particles, which corroborates the results obtained using XRD. The two Cu-*K*α and Cu-*K*β reflections present in Fig. 4 are artefacts due to the Cu support (which is commonly used in TEM studies) producing intense X-ray fluorescence even if Cu is not present in the sample.

This predominance of particles around the fibres is due to the long-chain amine precursor (DDA) generating more silica around the Pal-T fibres compared to the BTA co-surfactant.

Textural analysis

The textural properties of this type of heterostructured material provide important information regarding the nanoarchitecture produced. The SSA and microporous and mesoporous volume data before and after modification of Pal-T determined from the nitrogen adsorption isotherm at −196°C are collected in Table 1.

Pal exhibited a type-IV isotherm (not shown). This adsorption isotherm is generally obtained with mesoporous adsorbents in which capillary condensation occurs at the greatest relative

https://doi.org/10.1180/clm.2023.6 Published online by Cambridge University Press

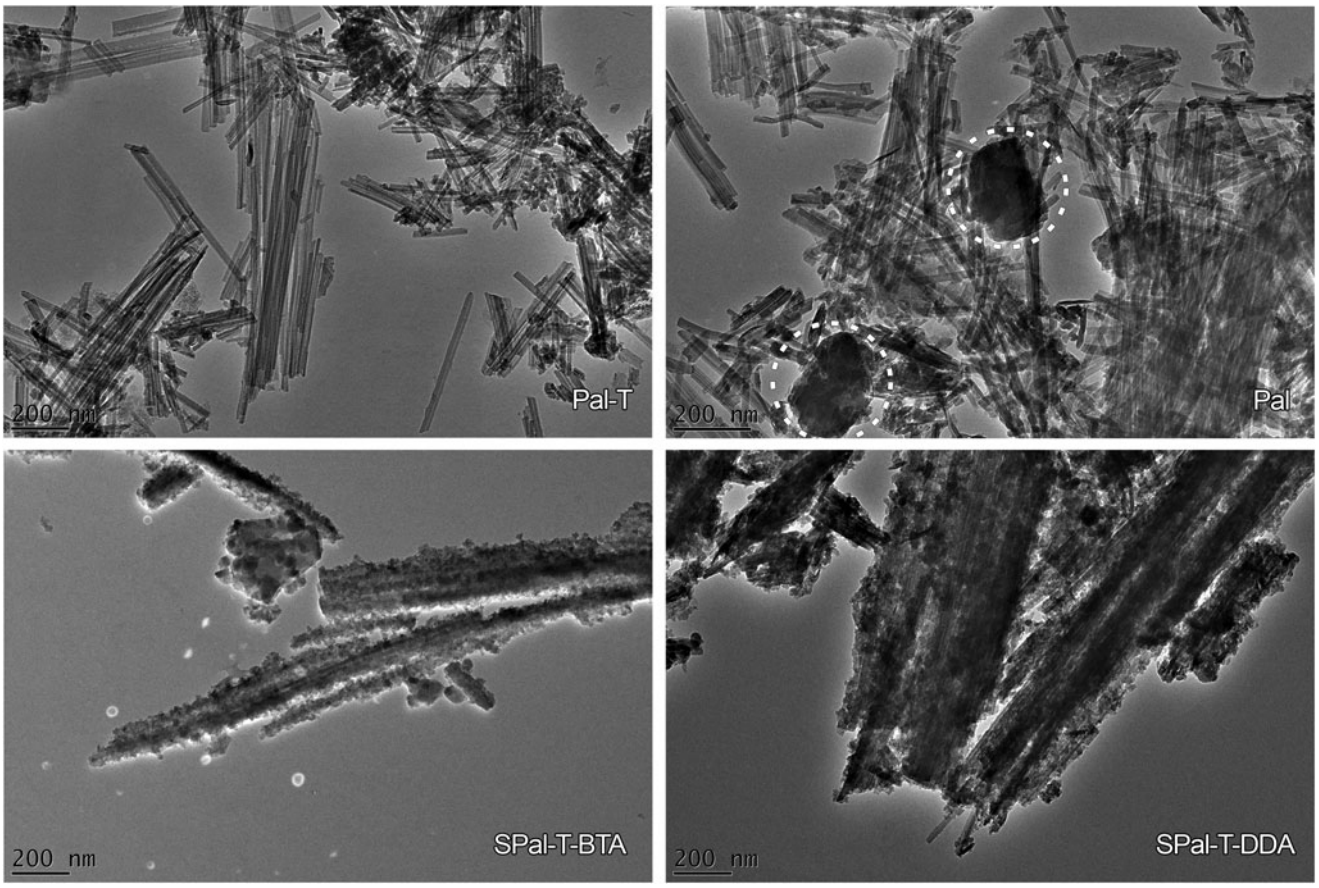

Fig. 3. TEM images showing raw palygorskite (Pal), activated palygorskite (Pal-T), a silica–palygorskite heterostructure obtained with co-surfactant BTA (SPal-T-BTA) and a silica–palygorskite heterostructure obtained with co-surfactant DDA (SPal-T-DDA). The dashed circle highlights the cubic crystals.

pressures. The raw Pal sample had a SSA value of ~87 m^2 g^{-1}. According to the data shown in Table 1, the raw sample was essentially mesoporous and not very microporous.

During acid purification, the mesoporous volume created in the clay mineral matrix (V_{meso} = 0.6 cm^3 g^{-1}) as well as the microporosity and ultramicroporosity increased significantly (V_{micro} = 0.027 cm^3 g^{-1}, V_{ultra} = 0.12 cm^3 g^{-1}), increasing the SSA from 87 m^2 g^{-1} before treatment to 302 m^2 g^{-1} after treatment. Thus, acid activation enabled fibre dissociation (as shown in the TEM images) in the raw Pal through carbonate removal (as confirmed by XRD analysis) as well as the removal of exchangeable cations, leading to the creation of new types of porosity, as has been reported previously (Suarez Barrios *et al.*, 1995; Boudriche *et al.*, 2011).

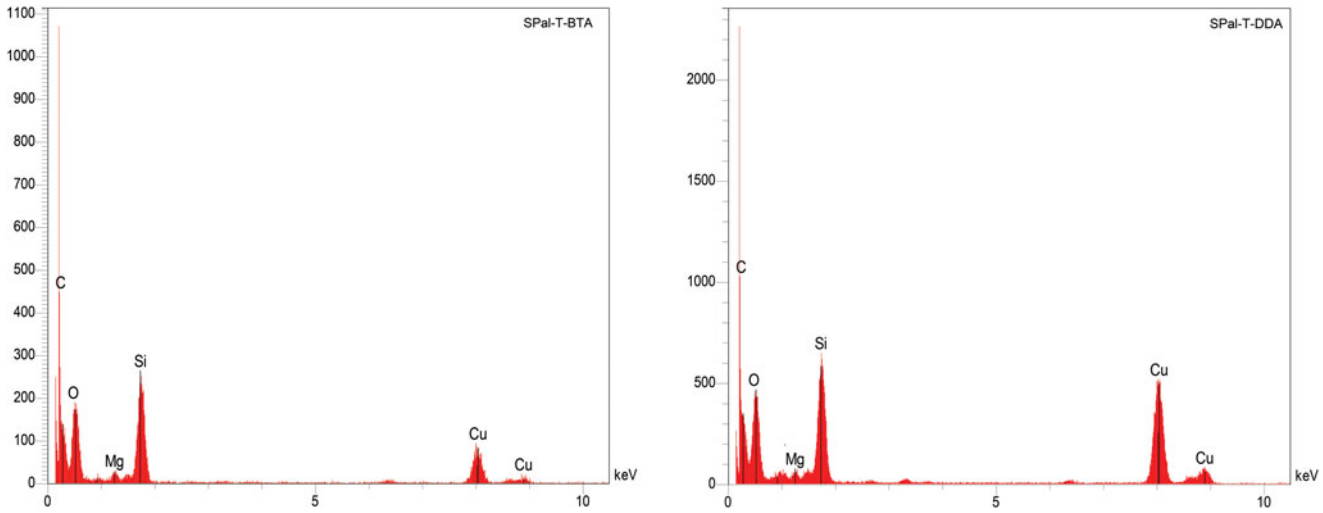

Fig. 4. EDX analysis of fibres in SPal-T-BTA and SPal-T-DDA.

https://doi.org/10.1180/clm.2023.6 Published online by Cambridge University Press

Table 1. Textural parameters of raw palygorskite (Pal), activated palygorskite (Pal-T) and the silica–palygorskite heterostructures SPal-T-BTA, SPal-T-DDA, SPal-BTA and SPal-DDA.

Sample	$V_{ultra\ (CO2)}$ DR ($cm^3\ g^{-1}$)	V_{N2} DR ($cm^3\ g^{-1}$)	SSA BET ($m^2\ g^{-1}$)	V_{micro} DFT ($cm^3\ g^{-1}$)	V_{meso} DFT ($cm^3\ g^{-1}$)
Pal	0.0225	0.0334	87	0.0014	0.2421
Pal-T	0.1232	0.1113	302	0.0279	0.5921
SPal-T-BTA	0.1134	0.1154	263	0.0731	0.1144
SPal-T-DDA	0.1811	0.2442	628	0.1165	0.2847
SPal-BTA	0.0914	0.0798	210	0.0293	0.2136
SPal-DDA	0.0796	0.0734	190	0.0384	0.2656

BET = Brunauer–Emmett–Teller.

After calcination, the greatest SSA was found for the SPal-T sample prepared from OPal-T/DDA/TEOS, at a value of 628 $m^2\ g^{-1}$ compared to a value of 263 $m^2\ g^{-1}$ for OPal-T/BTA/TEOS. This significant increase in SSA in SPal-T-DDA was attributed mainly to the new microporosity generated by the removal of the DDA surfactant from the micellar structure after calcination. However, the mesoporosity decreased significantly after calcination, causing volume losses of 48% and 30% with BTA and DDA co-surfactants, respectively. The hollow silicate spheres derived from the micellar structure after calcination were located specifically in the mesoporous volumes of the clay mineral with the short-chain co-surfactant BTA. These varying textural behaviours of the polymerized silica SiO_2 in the two SPal-T samples allow us to conclude that, after calcination, the co-surfactants used demonstrate varying levels of growth of the polysiloxane network around the fibres. Similar observations on the significant effects of various experimental variables, such as nature of both the alkoxysilane precursor and organo-sepiolite on the organization of the silica nanoparticles generated around the sepiolite fibres, have been reported previously by Gómez-Avilés *et al.* (2013).

To verify the contribution of decarbonation in the synthesis step, textural analysis of two other SPal samples was performed using raw non-activated Pal as starting material and BTA/DDA, respectively, as surfactants. From the SSA and porosity values (Table 1), and in contrast to the activated clay mineral, the values obtained with the two silica–palygorskite heterostructures – SPal-DDA and SPal-BTA – were of the same order of magnitude and remained significantly lower than the values obtained with Pal-T.

Thus, the acid activation in the presence of the short-chain co-surfactant (BTA) or the use of the long-chain co-surfactant (DDA) without acid activation were not sufficient to develop the porous network optimally; only the combination of long-chain co-surfactant and acid treatment allowed the optimization of the synthesis conditions of SPal. This combination played an important role in the organization of the silica precursor, leading to the creation of this new porous network consisting, in particular, of micropores and ultramicropores, which contribute significantly to the increase in specific surface area, as shown by the values obtained for the SPal-T-DDA sample (Table 1).

However, no differences were found between the XRD traces and FTIR spectra of the SPal-T-BTA and SPal-T-DDA samples and those of the SPal-BTA and SPal-DDA samples, respectively. The XRD and FTIR analyses of the samples obtained from raw Pal are not shown in Figs 2 & 5.

Chemical structure

The structural evolutions of Pal before and after acid activation and then after silica–palygorskite heterostructure formation are given in Fig. 5a,b in the spectral ranges of 4000–2600 and 2000–400 cm^{-1}, respectively.

The identification of Pal bands before modification was carried out by analogy with other studies conducted previously on similar types of fibrous clay minerals (Blanco *et al.*, 1989; Chahi *et al.*, 2002; Garcia-Romero *et al.*, 2004; Suarez *et al.*, 2006).

In the region of the vibrational bands of hydroxyl groups (Fig. 5a), a broad absorption band was detected between 3800 and 3000 cm^{-1}, with three distinguishable bands at 3620, 3560 and 3400 cm^{-1} and with a small shoulder at 3260 cm^{-1}.

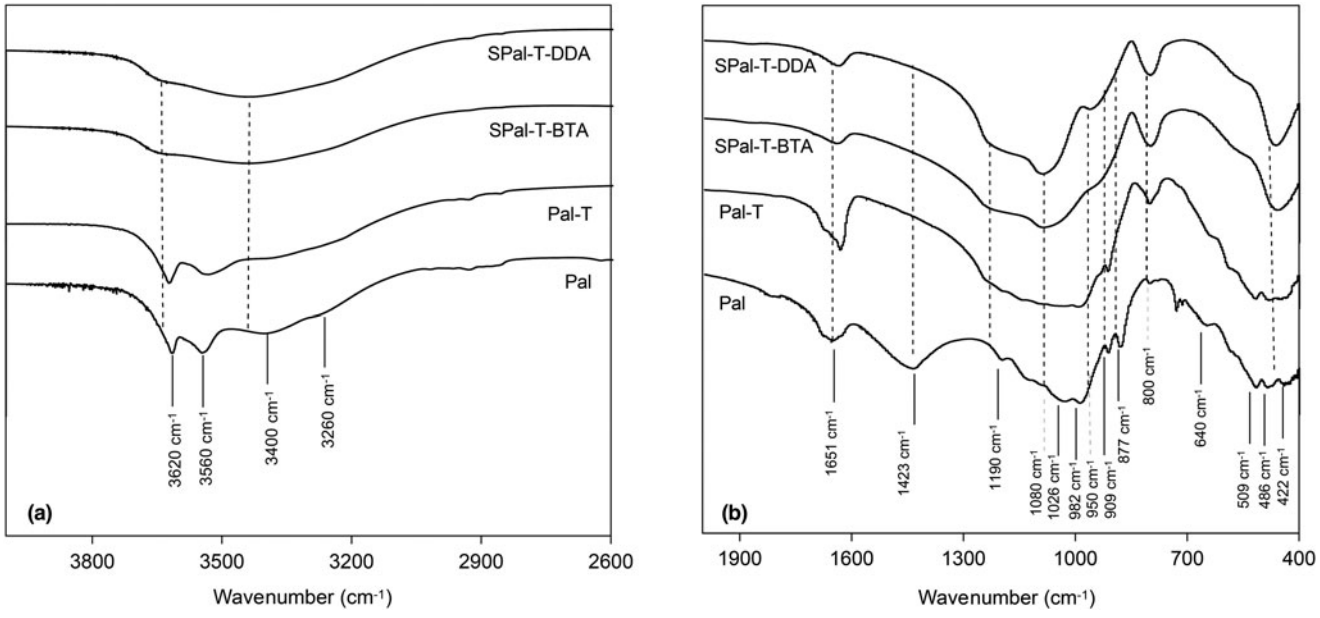

Fig. 5. FTIR spectra in the ranges (a) 4000–2600 cm^{-1} and (b) 2000–400 cm^{-1} of raw palygorskite (Pal), activated palygorskite (Pal-T) and the silica–palygorskite heterostructures SPal-T-BTA and SPal-T-DDA.

https://doi.org/10.1180/clm.2023.6 Published online by Cambridge University Press

The band at 3620 cm^{-1} was attributed to the OH-stretching vibration associated with Al^{3+} cations in dioctahedral coordination (Al_2OH) and the Mg-coordinated OH-stretching vibration of water along the fibres.

The band at 3560 cm^{-1} was attributed to the contribution of OH-stretching vibrations in (Fe,Mg)-OH and (Al,Mg)-OH.

The absorption band, with a maximum located at 3400 cm^{-1}, corresponded to the vibration of physisorbed water that interacted with the hydrogen atoms located at the edge of the fibres (these hydrogens have the role of compensating for the charge deficits due to edge effects).

After calcination, in the SPal spectra a single broad complex band centred at 3440 cm^{-1} appeared along with a band towards 3650 cm^{-1} due to dehydroxylation (1) with the release of the less stable OH groups that are bound mainly to aluminium and magnesium and (2) with the removal of coordinated, zeolitic and crystallization water molecules during the calcination step (Boudriche *et al.*, 2012).

In the region from 2000 to 400 cm^{-1} in Fig. 5b, the bands at 1423 and 877 cm^{-1} in the raw Pal related to carbonate impurities (vibrations of the CO_3^{2-} moiety) disappeared after acid activation, confirming the dissolution of these impurities (Suarez Barrios *et al.*, 1995; Boudriche *et al.*, 2011; Habibi *et al.*, 2018), as evidenced by the XRD analysis.

An intense H_2O deformation band appeared at ~1651 cm^{-1}. This band decreased sharply in intensity in the SPal spectra, corroborating the removal of bound and zeolitic water molecules after calcination.

The bands at 1190, 1026 and 982 cm^{-1} are attributable to the elongation vibrations of the Si–O–Si bond (Mendelovici, 1973; Gonzalez *et al.*, 1989) in the tetrahedral sheets in raw Pal, and these bands appeared in the SPal spectra as a new band centred at 1080 cm^{-1}, characteristic of asymmetric stretching vibrations of Si–O–Si bridges. In addition, two other distinct bands appeared at 1210 and 1080 cm^{-1}, characteristic of the presence of SiO_2 nanoparticles in hybrid structures such as SPal (Olejniczak *et al.*, 2005; Gómez-Avilés *et al.*, 2013).

A new band appeared at 800 cm^{-1} in SPal, attributable to symmetric stretching vibrations of Si–O bridges in the silica formed (Gonzalez *et al.*, 1989; Suarez Barrios *et al.*, 1995; Olejniczak *et al.*, 2005). This band appeared in the spectrum of Pal-T (Gonzalez *et al.*, 1989; Boudriche *et al.*, 2011) and then increased in intensity in the final calcined samples (SPal-T-BTA, SPal-T-DDA), indicating the additional contribution of the silica formed by polymerization of TEOS and thus confirming the formation of the mesoporous structure. Upon addition of the co-surfactant (DDA/BTA) and a Si source (TEOS) to the OPal-T sample, a broad Si–O complex band at 1080 cm^{-1} appeared, indicating the hydrolysis of TEOS and the development of a silica network in the SPal precursor. Another band also appeared at 950 cm^{-1}, attributable to the deformation vibration of silanol groups bound to the formed silica (Mendelovici, 1973; Gonzalez *et al.*, 1989; Olejniczak *et al.*, 2005). This band was more appreciable in SPal-T-DDA.

The 909 cm^{-1} band before treatment disappeared in the SPal spectra due to the release of the less stable OH groups that are bound mainly to aluminium and magnesium during calcination (Palkova *et al.*, 2010).

In the short-wavelength region of the SPal spectra, the intense band at ~455 cm^{-1} was attributed to the bending vibration of Si–O bridges in the silica formed (Olejniczak *et al.*, 2005).

The SPal-T-DDA sample, which presents the most advantageous textural properties (great SSA and developed porous network), will be tested for its use in air-pollution control and for the elimination of volatile organic compounds at low concentrations, in particular toluene and decane, in order to evaluate its adsorption capacity.

Conclusion

The preparation of heterostructured materials based on the immobilization of silica on a clay mineral, palygorskite, was carried out by varying two experimental conditions: (1) the acid activation of the clay mineral and (2) the neutral amine chain length. The mineralogical and structural analyses of the samples obtained demonstrated the formation of amorphous silica on the surface of the palygorskite fibres with preservation of the fibrous structure. This result is confirmed by the morphological analysis, which indicates total coverage of the surface of the palygorskite fibres by silica nanoparticles. Moreover, gas adsorption proved to be the most relevant analysis technique, as it revealed that the use of acid-activated clay minerals combined with a long-chain neutral amine co-surfactant optimized the textural properties of the formed silica–palygorskite heterostructure. The SSA and porosity measurements demonstrated that the SPal-T-DDA sample compared to the other heterostructures had a highly developed pore network ($V_{N2} = 0.24$ cm^3 g^{-1}; $V_{ultra\ (CO2)} = 0.18$ cm^3 g^{-1}) with a high SSA (628 m^2 g^{-1}). These results confirm that the textural characteristics of the heterostructure obtained after removal of the organic matter and consolidation of the silica network on the external surface depend significantly on the experimental conditions used. Controlling such preparation conditions enables diversification of the physicochemical properties of the nanoarchitectures obtained, leading to a multitude of application possibilities.

References

Akkari M., Aranda P., Ben Haj Amara A. & Ruiz-Hitzky E. (2018) Clay-nanoarchitectures as photocatalysts by in situ assembly of ZnO nanoparticles and clay minerals. *Journal of Nanoscience and Nanotechnology*, **18**, 223–233.

Aranda P. & Ruiz-Hitzky E. (2018) Immobilization of nanoparticles on fibrous clay surfaces: towards promising nanoplatforms for advanced functional applications. *Chemical Record*, **18**, 1125–1137.

Belaroui L. S., Ouali A., Bengueddach A., Lopez Galindo A. & Peña A. (2018) Adsorption of linuron by an Algerian palygorskite modified with magnetic iron. *Applied Clay Science*, **164**, 26–33.

Belver C., Aranda P., Martín-Luengo M. A. & Ruiz-Hitzky E. (2012) New silica/alumina–clay heterostructures: properties as acid catalysts. *Microporous and Mesoporous Materials*, **147**, 157–166.

Belver C., Aranda P. & Ruiz-Hitzky E. (2013) Silica–alumina/sepiolite nanoarchitectures. *Journal of Material Chemistry A*, **1**, 7477–7487.

Blanco C., Gonzalez F., Pesquera C. & Benito I. (1989) Differences between one aluminic palygorskite and another magnesic by infrared spectroscopy. *Spectroscopy Letters*, **6**, 659–673.

Boudriche L., Hamdi B., Kessaissia Z., Calvet R., Chamayou A., Dodds J. D. & Balard. H. (2010) Assessment of the surface properties of milled palygorskite using inverse gas chromatography. *Clays and Clay Minerals*, **58**, 143–153.

Boudriche L., Calvet R., Hamdi B. & Balard H. (2011) Effect of acid treatment on surface properties evolution of palygorskite clay: an application of inverse gas chromatography. *Colloids and Surfaces A: Physicochemical and Engineering Aspects*, **392**, 45–54.

Boudriche L., Calvet R., Hamdi B. & Balard H. (2012) Surface properties evolution of palygorskite by IGC analysis as a function of thermal treatment. *Colloids and Surfaces A: Physicochemical and Engineering Aspects*, **399**, 1–10.

Bradley W.F. (1940) The structural scheme of palygorskite. *American Mineralogist*, **25**, 405–410.

https://doi.org/10.1180/clm.2023.6 Published online by Cambridge University Press

Cecilia J.A., Garcıa-Sancho C., Vilarrasa-Garcıa E., Jimenez-Jimenez J. & Rodriguez-Castellon E. (2018) Synthesis, characterization, uses and applications of porous clays heterostructures: a review. *Chemical Record*, **18**, 1–21.

Chahi A., Petit S. & Decarreau A. (2002) Infrared evidence of dioctahedral–trioctahedral site occupancy in palygorskite. *Clays and Clay Minerals*, **50**, 306–313.

Dai F., Guo J., He Y., Song P. & Wang R. (2021) Enhanced thermal stability and adsorption performance of MIL-53(Fe)@ montmorillonite. *Clay Minerals*, **56**, 99–107.

García-Romero E., Suárez-Barrios M. & Bustillo-Revuelta M.A. (2004) Characteristics of a Mg-palygorskite in Miocene rocks, Madrid Basin (Spain). *Clays and Clay Minerals*, **52**, 484–494.

Gómez-Avilés A., Aranda P., Fernandes F.M., Belver C. & Ruiz-Hitzky E. (2013) Silica–sepiolite nanoarchitectures. *Journal of Nanoscience and Nanotechnology*, **13**, 2897–2907.

González-Alfaro Y., Aranda P., Fernandes F.M., Wicklein B., Darder M. & Ruiz-Hitzky E. (2011) Multifunctional porous materials through ferrofluids. *Advanced Materials*, **23**, 5224–5228.

Gonzalez F., Pesquera C., Blanco C., Benito I., Mendioroz S. & Pajares J. A. (1989) Structural and textural evolution of Al- and Mg-rich palygorskites, I. Under acid treatment. *Applied Clay Science*, **4**, 373–388.

Guggenheim S. & Krekeler M.P.S. (2011) The structure and microtextures of the palygorskite–sepiolite group minerals. Pp. 3–32 in: *Developments in Palygorskite–Sepiolite Research. A New Outlook on These Nanomaterials* (E. Galan & A. Singer, editors). Elsevier BV, Oxford.

Habibi A., Belaroui L.S., Bengueddach A., López Galindo A., Sainz Díaz C.I. & Peña A. (2018) Adsorption of metronidazole and spiramycin by an Algerian palygorskite. Effect of modification with tin. *Microporous and Mesoporous Materials*, **268**, 293–302.

Kooli F., Liu Y., Hbaieb K. & Al-Faze R. (2017) Preparation and catalytic activities of porous clay heterostructures from aluminium-intercalated clays: effect of Al content. *Clay Minerals*, **52**, 521–535.

Mendelovici E. (1973) Infrared study of palygorskite and HCl treated palygorskite. *Clays and Clay Minerals*, **21**, 115–119.

Olejniczak Z., Leczka M., Cholewa-Kowalska K., Wojtach K., Rokita M. & Mozgawa W. (2005) ^{29}Si MAS NMR and FTIR study of inorganic–organic hybrid gels. *Journal of Molecular Structure*, **744**, 465–471.

Ouali A., Belaroui L.S., Bengueddach A., Galindo A.L. & Peña A. (2015) Fe_2O_3–palygorskite nanoparticles, efficient adsorbates for pesticide removal. *Applied Clay Science*, **115**, 67–75.

Palkova H., Madejova J., Zimowska M. & Serwicka E.M. (2010) Laponite-derived porous clay heterostructures: II. FTIR study of the structure evolution. *Microporous and Mesoporous Materials*, **127**, 237–244.

Persano F., Gigli G. & Leporatti S. (2021) Halloysite-based nanosystems for biomedical applications. *Clays and Clay Minerals*, **69**, 501–521.

Polverejan M., Pauly T.R. & Pinnavaia T.J. (2000) Acidic porous clay heterostructures (PCH): intragallery assembly of mesoporous silica in synthetic saponite clays. *Chemical Materials*, **12**, 2698–2704.

Ruiz-Hitzky E. & Aranda P. (2014) Novel architectures in porous materials based on clays. *Journal of Sol-Gel Science and Technoogy*, **70**, 307–316.

Ruiz-Hitzky E., Aranda P., Alvarez A., Santaren J. & Cubillo A.E. (2011) Advanced materials and new applications of sepiolite and palygorskite. *Developments in Clay Science*, **3**, 393–452.

Suarez M. & Garcia-Romero E. (2006) FTIR spectroscopic study of palygorskite: influence of the composition of the octahedral sheet. *Applied Clay Science*, **31**, 154–163.

Suarez Barrios M., Flores Gonzalez L.V., Vicente Rodriguez M.A. & Martin Pozas J.M. (1995) Acid activation of a palygorskite with HCl: development of physico-chemical, textural and surface properties. *Applied Clay Science*, **10**, 247–258.

Tobajas M., Belver C. & Rodriguez J.J. (2017) Degradation of emerging pollutants in water under solar irradiation using novel TiO_2-ZnO/clay nanoarchitectures. *Chemical Engineering Journal*, **309**, 596–606.

Yang H., Tang A., Ouyang J., Li M. & Mann S. (2010) From natural attapulgite to mesoporous materials: methodology, characterization and structural evolution. *Journal of Physical Chemistry B*, **114**, 2390–2398.

Yang P., Song M., Kim D., Jung S.P. & Hwang Y. (2019) Synthesis conditions of porous clay heterostructure (PCH) optimized for volatile organic compounds (VOC) adsorption. *Korean Journal of Chemical Engineering*, **36**, 1806–1813.

Yuan M., Deng W., Dong S., Li Q., Zhao B. & Su Y. (2018) Montmorillonite based porous clay heterostructures modified with Fe as catalysts for selective catalytic reduction of NO with propylene. *Chemical Engineering Journal*, **353**, 839–848.

https://doi.org/10.1180/clm.2023.6 Published online by Cambridge University Press